Eur. Phys. J. B **28**, 111–115 (2002)
DOI: 10.1140/epjb/e2002-00206-x

THE EUROPEAN PHYSICAL JOURNAL B

Characterization of Bernstein modes in quantum dots

M. Valín-Rodríguez[1], A. Puente[1], L. Serra[1,a], V. Gudmundsson[2], and A. Manolescu[2]

[1] Departament de Física, Universitat de les Illes Balears, 07071 Palma de Mallorca, Spain
[2] Science Institute, University of Iceland, Dunhaga 3, 107 Reykjavik, Iceland

Received 3 December 2001 / Received in final form 5 April 2002
Published online 9 July 2002 –

Abstract. The dipole modes of non-parabolic quantum dots are studied by means of their current and density patterns as well as with their local absorption distribution. The anticrossing of the so-called Bernstein modes originates from the coupling with electron-hole excitations of the two Landau bands which are occupied at the corresponding magnetic fields. Non-quadratic terms in the potential cause an energy separation between bulk and edge current modes in the anticrossing region. On a local scale the fragmented peaks absorb energy in complementary spatial regions which evolve with the magnetic field.

PACS. 73.21.-b Electron states and collective excitations in multilayers, quantum wells, mesoscopic and nanoscale systems – 73.20.Mf Collective excitations (including excitons, polarons, plasmons and other charge-density excitations)

1 Introduction

The far infrared (FIR) spectroscopy has proved to be an invaluable tool for the physical characterization of semiconductor quantum dots and other electronic nanostructures [1,2]. Since its initial applications to 2D semiconductor quantum dots one of the main motivations has been to identify a signal of the relative motion of the confined electrons. As is well known [3], most commonly the confinement seems to be parabolic, and in this limit the generalized Kohn theorem assures that the only allowed excitations are the center-of-mass modes, at the frequencies

$$\omega_{\pm}(B) = \sqrt{\omega_0^2 + \frac{\omega_c^2}{4}} \pm \frac{\omega_c}{2} \,, \tag{1}$$

where B is the applied perpendicular magnetic field, ω_0 is the frequency associated with the external parabola and $\omega_c = eB/c$ is the cyclotron frequency [4].

In reference [5] the fragmentation of the high-energy branch $\omega_+(B)$ was measured in wires and dots and interpreted as an interaction with the cyclotron harmonics at energies $n\omega_c$ ($n = 2, 3$). Since these interactions resemble the Bernstein modes of the electron gas [6], the same name was used to label the corresponding excitations in these nanostructures. More recently, Krahne *et al.* [7] have measured the Bernstein modes in a 2D GaAs system with tunable electron density, varying from a continuous 2D gas to well separated dots. While the anticrossing exactly occurs at $2\omega_c$ for the 2D gas, for finite quantum dots it lies below (between ω_c and $2\omega_c$).

It is our aim in this paper to provide a physical characterization of the below-$2\omega_c$ Bernstein modes of quantum dots by analysing the current and density distributions, as well as the local absorption patterns, associated with each particular peak of the dipole spectrum. For this purpose, we shall use the time-dependent local-spin-density approximation in a symmetry unrestricted formalism as developed recently in reference [8]. A comparison with the electron-hole interband transitions will also shed light on the origin of the fragmentation of the $\omega_+(B)$ branch.

2 Theoretical approach

As in reference [5] we assume the following confining potential

$$v_{\rm conf}(r) = \frac{1}{2}\omega_0 \left[\left(\frac{r}{\ell_0}\right)^2 + a \left(\frac{r}{\ell_0}\right)^4 \right] \,, \tag{2}$$

with r the radial coordinate in the xy plane, where the electronic motion occurs, $\ell_0 = \omega_0^{-1/2}$ the *confining length*, $\omega_0 = 3.37$ meV and $a = 2.02 \times 10^{-2}$. The parameter a controls the degree of non-parabolicity although, as shown in reference [5], the Bernstein fragmentation discussed below is actually not much sensitive on its precise value. It is worth to mention that a similar potential including a quartic term was used by Ye and Zaremba to analyze the breaking of Kohn's theorem in the context of a hydrodynamic approach [9].

We assume the effective-mass Hamiltonian, applicable to GaAs nanostructures [10], and describe the electronic exchange and correlation effects within the Local-Spin-Density approximation (LSDA). This density-functional approach has recently been used by several authors to describe quantum dot properties. The reader is addressed to

[a] e-mail: dfslsc4@clust.uib.es

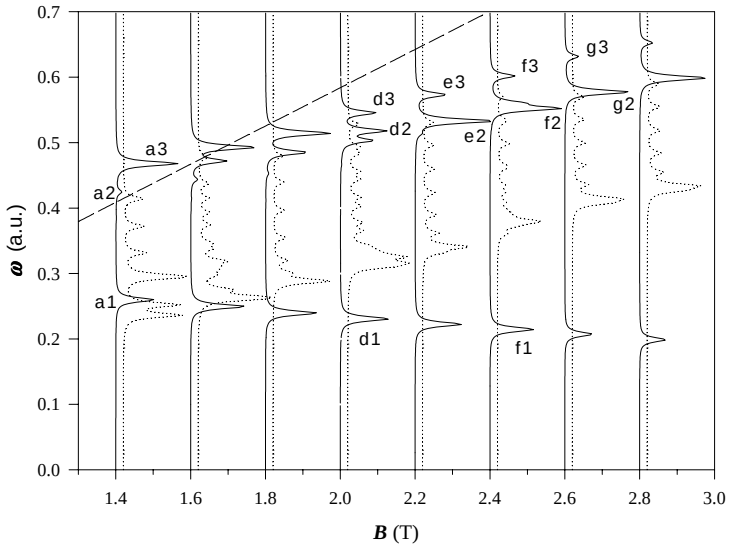

Fig. 1. Evolution of the dipole strength for the 20-electron dot. The dashed line indicates $\omega = 2\omega_c$ and the dotted one the $\Delta\ell = +1$ electron-hole interband transitions. The labels identify the different peaks discussed in the text.

references [11–13] for details on the method. In the context of the FIR absorption the time-dependent extension (TDLSDA) has also been shown to provide adequate results [14,15].

The dynamical properties described below have been calculated by integrating the Kohn-Sham equations

$$\mathrm{i}\frac{\partial\varphi_{i\eta}(\mathbf{r},t)}{\partial t} = h_\eta[\rho,m]\;\varphi_{i\eta}(\mathbf{r},t)\;, \tag{3}$$

where $\eta = \uparrow,\downarrow$ labels the two spin components, while $\rho = \sum_{\mathrm{occ.}} |\varphi_{i\uparrow}|^2 + |\varphi_{i\downarrow}|^2$ indicates the total particle density and $m = \sum_{\mathrm{occ.}} |\varphi_{i\uparrow}|^2 - |\varphi_{i\downarrow}|^2$ the total spin magnetization. The self-consistent Hamiltonian in equation (3) reads

$$\begin{aligned} h_\eta[\rho,m] &= \frac{1}{2}\left(-\mathrm{i}\nabla + \frac{e}{c}\mathbf{A}(\mathbf{r})\right)^2 + v_{\mathrm{conf}}(r) \\ &+ \int \mathrm{d}\mathbf{r}'\,\frac{\rho(\mathbf{r}')}{|\mathbf{r}-\mathbf{r}'|} + \frac{\delta E_{XC}[\rho,m]}{\delta\rho} \\ &+ s_\eta\left(\frac{\delta E_{XC}[\rho,m]}{\delta m} + g^*\mu_B\frac{B}{2}\right)\;, \end{aligned} \tag{4}$$

with $\mathbf{A}(\mathbf{r}) = B/2(-y,x)$ being the vector potential in the symmetric gauge, $E_{XC}[\rho,m]$ the exchange-correlation functional, and $s_\eta = \pm 1$ for $\eta = \uparrow,\downarrow$, respectively. The Zeeman term in equation (4) contains the gyromagnetic factor g^* and the Bohr magneton $\mu_B = e/2m_e c$.

3 Single peak analysis

After calculating the ground state structure and in order to excite the collective dipole mode we perform a small rigid translation of the electronic cloud. This takes the system out of equilibrium and as a consequence it begins to oscillate. The expectation values of several observables $\mathcal{O}$ are subsequently recorded in time $\langle\mathcal{O}\rangle(t)$ and frequency analysed to obtain the corresponding energy distributions. In the present analysis we have considered the dipole, local current and local density operators, *i.e.*,

$$\begin{aligned} \hat{D} &= \sum_i x_i + y_i\;, \\ \hat{\mathbf{j}}(\mathbf{r}) &= \sum_i \left[-\frac{i}{2}\left(\overrightarrow{\nabla}_i - \overleftarrow{\nabla}_i\right) + \frac{e}{c}\mathbf{A}(\mathbf{r}_i)\right]\delta(\mathbf{r}-\mathbf{r}_i)\;, \\ \hat{\rho}(\mathbf{r}) &= \sum_i \delta(\mathbf{r}-\mathbf{r}_i)\;. \end{aligned} \tag{5}$$

Note that after the frequency analysis we obtain $\langle\mathcal{O}\rangle(\omega)$ which for the local signals provides a pattern of currents $\langle\hat{\mathbf{j}}(\mathbf{r})\rangle(\omega)$ and of local density $\langle\hat{\rho}(\mathbf{r})\rangle(\omega)$ that can obviously be ascribed to the excitation at energy ω. At a fixed ω, the time evolution at every point $\mathbf{r}$ is simply given by a phase $\mathrm{e}^{-\mathrm{i}\omega t}$, or by $\sin(\omega t)$ and $\cos(\omega t)$ for the corresponding real transforms, thus permitting to monitor the variation of the current and density patterns for each excitation peak. In addition, the density patterns can be used to obtain the local absorption from $|\,\langle\hat{\rho}(\mathbf{r})\rangle(\omega)\,|$, as done in reference [16] for the characterization of the FIR absorption of triangular and square quantum dots. Theoretically, the local absorption at $\mathbf{R}$ provides the energy absorbed by the system when a probe of the type $\xi(\mathbf{r}-\mathbf{R})$ is used, where ξ is a highly peaked spatial modulation [17]. Note also that in equation (5) we have used the gauge invariant current including explicitly the vector potential $\mathbf{A}(\mathbf{r})$.

4 Results

Figure 1 displays the FIR absorption for a dot with $N = 20$ electrons in the confining potential (2) for different vertical magnetic fields. The Bernstein fragmentation of the high energy branch is conspicuous for $1.6\ \mathrm{T} < B < 2.4\ \mathrm{T}$. Actually, for several B's up to three

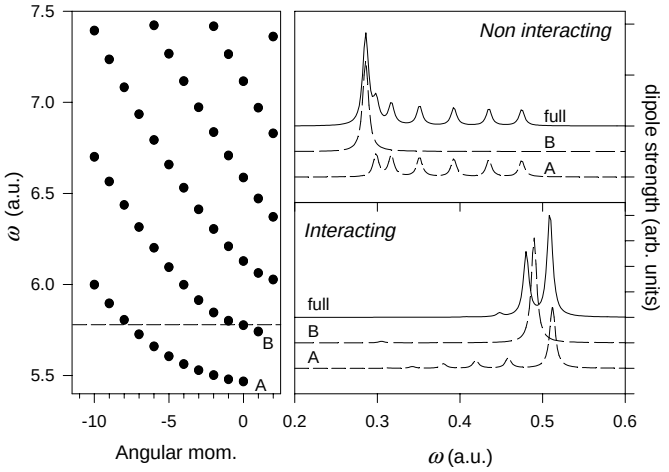

Fig. 2. Left panel displays the Kohn-Sham single particle energies as a function of angular momentum at a magnetic field $B = 1.8$ T. The dashed line separates occupied and non-occupied levels. Right panels show the response using the perturbative approach [18]. The dashed lines correspond to the restricted subspaces for hole states in Landau bands A and B, respectively.

peaks can be identified in the higher branch, although in most instances this branch fragments into two dominant features. In this figure the dashed line indicates the $2\omega_c$ values while the dotted lines show the particle-hole transitions with $\Delta\ell = +1$, which by angular-momentum selection rules are the only ones that couple to the high-energy branch. All these transitions are of interband character. The $\Delta\ell = -1$ particle-hole transitions (of both intra- and interband character) only contribute to the low-energy branch and thus are not relevant for the present discussion. From this figure and the results that will be presented below, the fragmentation of the FIR absorption, causing the Bernstein modes, can be understood as an effect of the coupling with particle-hole transitions, allowed by the non-parabolicity of the confining potential. Note that at $B \approx 2$ T there is a particle-hole excitation actually lying in between the fragmented Bernstein peaks, thus showing that the maximal overlap of the interacting response with the interband transitions occurs below the $2\omega_c$ line. We stress that in spite of the overlap with $\omega_-(B)$, the displayed transitions do not couple with the lower branch by angular momentum selection rules.

The relevance of the different particle-hole transitions is more easily appreciated within the perturbative response formalism, as opposed to the real-time one (see, *e.g.*, Ref. [18]). Using the perturbative method, in Figure 2 we compare the full absorption function at $B = 1.8$ T with those obtained by including only the hole states from the first and second Landau bands, respectively, shown in the left panel. The interacting responses in the restricted subspaces show collective peaks which approximately reproduce the energies of the Bernstein excitations in the full response. Therefore, each of the Bernstein peaks can be thought of as arising from particle-hole excitations of different bands, as it happens in the bulk limit for a modulated 2D gas [19]. Note, however, that the picture of separate FIR excitations for each band is an approximate one, since there are important interference effects between bands. With this interpretation we expect that when $\omega_+(B)$ and $2\omega_c(B)$ intersect in a region where only one Landau band is occupied there will be no Bernstein fragmentation as in Figure 1. Indeed we have checked this by using a much lower value of the confinement, $\omega_0 = 0.5$ meV, which for $B = 0.3$ T has one (spin degenerate) occupied Landau band and $\omega_+(B) \approx 2\omega_c(B)$ without any anticrossing.

The preceding analysis is in qualitative agreement with the results for Raman modes in quantum wires of Steinebach *et al.* [20]. These authors attribute the anticrossing to the large importance of transitions with $\Delta n = 2$, where n is the Landau level index, with respect to those with $\Delta n = 1$. Realizing that $\Delta n = 1$ transitions are mainly from the highest occupied Landau band, while $\Delta n = 2$ also includes the second highest Landau band, one arrives at a similar conclusion as the above one.

We consider next the current distributions. The pure Kohn modes in parabolic dots correspond to rigid translations of the electronic density and, therefore, to essentially uniform current distributions, the only variations being due to the density inhomogeneities. A similar result is found for the low energy branch in Figure 1, indicating the Kohn-like character of this mode.

The current patterns at a given time for the Bernstein modes in the nonparabolic dot are shown in Figure 3. The time evolution for each of these patterns is simply an anticlockwise rotation, in agreement with the $\Delta\ell = +1$ character of the mode (the positive z axis is pointing towards the reader). The leftmost panel corresponds to the dominant peak at $B = 1.4$ T, which displays a current pattern basically uniform in the bulk of the dot, thus similar to the previously mentioned Kohn modes. The two intermediate panels correspond to the peaks at $B = 2$ T (at $\omega \approx 0.52$ and 0.54). They show an incipient separation of bulk and edge current oscillations which is further developed at $B = 2.4$ T (two right panels). Note that the edge-current patterns contain a hole in the dot center. Therefore, the non-parabolicity of the potential induces a separation in energy of the higher-branch bulk and edge current modes, which are degenerate in the purely parabolic case.

It is also interesting to look at the density variation patterns displayed in Figure 4 for the $B = 2.4$ T case. As before, the time evolution of each pattern is a clockwise rotation for the lower-energy branch and anticlockwise for the upper modes. Plus and minus signs indicate increment and decrement in the local density, respectively. Note that both the low-energy peak (f1) and the dominant peak of the higher branch (f2) exhibit a simple dipole pattern with two lobes. On the contrary, the highest mode (f3) displays an internal structure reflecting the existence of a node in the radial density and four regions with alternate phases. The internal structure of f3 nicely correlates with the the current pattern of Figure 3, since the regions of current convergence

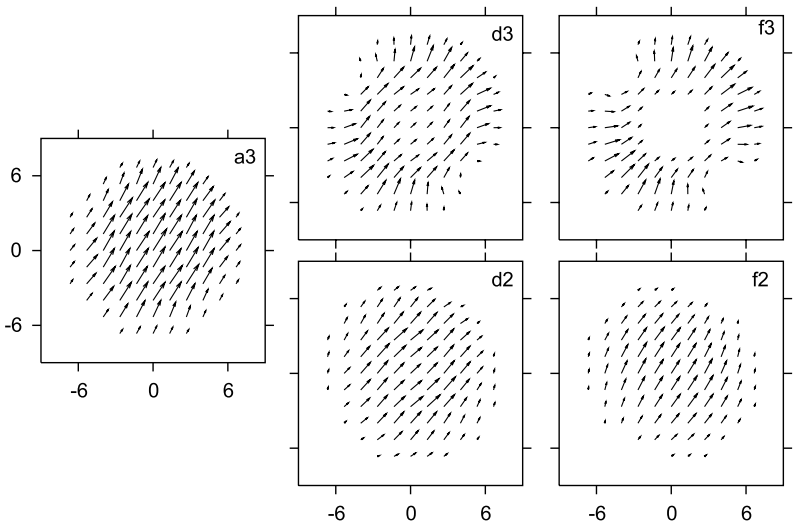

Fig. 3. Current density patterns for the high energy branch at different magnetic fields. Each label indicates the corresponding mode in Figure 1. A different absolute scale, varying in proportion to the dipole strength of the corresponding peak of Figure 1, has been used in each panel.

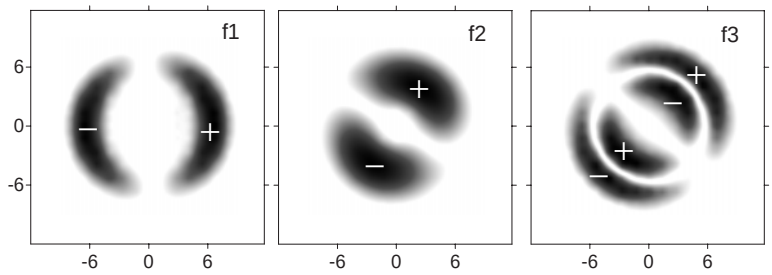

Fig. 4. Pattern of local-density variations for the indicated modes of Figure 1 which correspond to the three dipole peaks at $B = 2.4$ T. The gray color scale indicates the signal magnitude while the corresponding sign is superimposed in white.

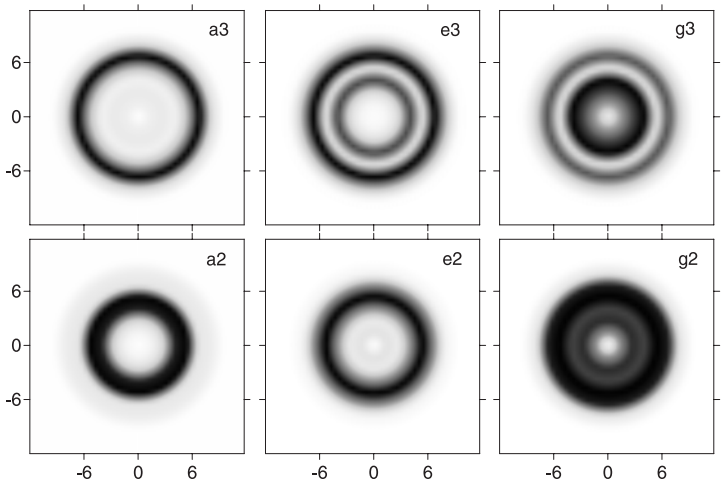

Fig. 5. Local absorption patterns for the Bernstein peaks at different magnetic fields. Black regions correspond to high absorption, with an absolute scale proportional to the peak's dipole strength.

(divergence) correspond to an increase (decrease) of the local density.

A time average of the oscillating density amplitudes highlights the regions of higher FIR absorption in the dot, as shown in Figure 5. The different grey colours indicate the absorption strength as given by the local oscillation. We notice that at $B = 1.4$ T the Bernstein peaks absorb basically in rings, with the lower peak having a more internal character. As the magnetic field is raised the lower peak tends to expand its absorption ring, while the higher one absorbs more in the inner region. As a result, at $B \approx 2.6$ T the two modes reverse their character, the upper mode becoming more internal. Thus showing that the two Bernstein peaks absorb energy in complememtary spatial regions.

5 Conclusions

We have analysed the fragmentation of the high-energy branch in non-parabolic dots by using a) a comparison with the allowed electron-hole transitions, b) the current and density variations associated with each peak, and c) the local absorption pattern of each mode. We conclude that the Bernstein fragmentation is a result of the coupling with electron-hole dipole transitions originating from each of the two occupied Landau bands. This coupling manifests in an energy separation of the bulk and edge current modes, with the latter one having a four-lobe structure in the oscillating density. The separation of the modes is also reflected in the local absorption, being more internal for the lower peak than for the higher one at small B's and reverting character when the magnetic field is increased.

This work was supported by Grant No. PB98-0124 from DGESeiC, Spain, the Research Fund of the University of Iceland, and the Icelandic Natural Science Council.

References

1. C. Sikorski, U. Merkt, Phys. Rev. Lett. **62**, 2164 (1989)
2. T. Demel, D. Heitmann, P. Grambow, K. Ploog, Phys. Rev. Lett. **66**, 2657 (1991)
3. L. Jacak, P. Hawrylak, A. Wójs, *Quantum dots* (Springer, 1998)
4. We use the effective-atomic-unit system in the context of the effective-mass Hamiltonian. In terms of the the semiconductor dielectric constant κ and electron effective mass m we thus impose $e^2/\kappa = m = \hbar^2 = 1$
5. V. Gudmundsson, A. Brataas, P. Grambow, B. Meurer, T. Kurth, D. Heitmann, Phys. Rev. B **51**, 17 744 (1995)
6. I.B. Bernstein, Phys. Rev. **109**, 10 (1958)
7. R. Krahne, M. Hochgräfe, Ch. Heyn, D. Heitmann, Phys. Rev. B **61**, 16 319 (2000)
8. A. Puente, Ll. Serra, Phys. Rev. Lett. **83** 3266 (1999)
9. Z.L. Ye, E. Zaremba, Phys. Rev. B **50**, 17217 (1994)
10. Taking the GaAs values for the electron effective mass $m = 0.0667m_e$, dielectric constant $\kappa = 12.4$ and electron giromagnetic factor $g^* = -0.44$, the associated effective atomic units are the modified Hartree $H^* \approx 12$ meV, and effective Bohr radius $a_0^* \approx 100$ Å.
11. M. Ferconi, G. Vignale, Phys. Rev. B **50**, 14722 (1994)
12. M. Koskinen, M. Manninen, S.M. Reimann, Phys. Rev. Lett. **79**, 1389 (1999)
13. K. Hirose, N.S. Wingreen, Phys. Rev. B **59**, 4604 (1999)
14. C.A. Ullrich, G. Vignale, Phys. Rev. B **61**, 2729 (2000)
15. A. Puente, Ll. Serra, Phys. Rev. B **63**, 125334 (2001)
16. M. Valín-Rodríguez, A. Puente, Ll. Serra, Phys. Rev. B **64**, 205307 (2001)
17. C.D. Simserides, U. Hohenester, G. Goldoni, E. Molinari, Phys. Rev. B **62**, 13657 (2000)
18. Ll. Serra, M. Barranco, A. Emperador, M. Pi, E. Lipparini, Phys. Rev. B **59**, 15290 (1999)
19. A. Manolescu, V. Gudmundsson, Phys. Rev. B **57**, 1668 (1998)
20. C. Steinebach, R. Krahne, G. Biese, C. Schüller, D. Heitmann, K. Eberl, Phys. Rev. B **54**, 14281 (1996)